

J. Hawke, R. Scannell, M. Maslov, J.B. Migozzi
and JET EFDA contributors

Spectral Calibration of the JET Core LIDAR Thomson Scattering Diagnostic Using Ray Tracing

“This document is intended for publication in the open literature. It is made available on the understanding that it may not be further circulated and extracts or references may not be published prior to publication of the original when applicable, or without the consent of the Publications Officer, EFDA, Culham Science Centre, Abingdon, Oxon, OX14 3DB, UK.”

“Enquiries about Copyright and reproduction should be addressed to the Publications Officer, EFDA, Culham Science Centre, Abingdon, Oxon, OX14 3DB, UK.”

The contents of this preprint and all other JET EFDA Preprints and Conference Papers are available to view online free at www.iop.org/Jet. This site has full search facilities and e-mail alert options. The diagrams contained within the PDFs on this site are hyperlinked from the year 1996 onwards.

Spectral Calibration of the JET Core LIDAR Thomson Scattering Diagnostic Using Ray Tracing

J. Hawke¹, R. Scannell², M. Maslov², J.B. Migozzi³
and JET EFDA contributors*

JET-EFDA, Culham Science Centre, OX14 3DB, Abingdon, UK

¹*FOM Institute DIFFER – Dutch Institute for Fundamental Energy Research,
Association EURATOM-FOM, 3430 BE Nieuwegein, Netherlands*

²*EURATOM-CCFE Fusion Association, Culham Science Centre, OX14 3DB, Abingdon, OXON, UK*

³*JBM Optique, 4 Rue du Calvaire Bâtiment 11, 92210 Saint Cloud, France*

** See annex of F. Romanelli et al, “Overview of JET Results”,
(24th IAEA Fusion Energy Conference, San Diego, USA (2012)).*

ABSTRACT

This work isolated the cause of the observed discrepancy between the electron temperature (T) measurements before and after the JET Core LIDAR Thomson Scattering (TS) diagnostic was upgraded. In the upgrade process, stray light filters positioned just before the detectors were removed from the system. Modelling showed that the shift imposed on the stray light filters transmission functions due to the variations in the incidence angles of the collected photons impacted plasma measurements. The shift in the stray light filter transmission function was examined for all channels of the JET Core LIDAR spectrometer. Due to proximity to the ruby laser wavelength and filter configuration, two of the diagnostics high wavelength channels were affected. To correct for this identified source of error, correction factors were developed using ray tracing models for the calibration and operational states of the diagnostic. The application of these correction factors resulted in an increase in the observed T, resulting in the partial if not complete removal of the observed discrepancy in the measured T between the JET core LIDAR TS diagnostic, High Resolution Thomson Scattering (HRTS), and the Electron Cyclotron Emission (ECE) diagnostics.

1. INTRODUCTION

Shortly into the ITER-like Wall (ILW) campaign [1,2] on JET, the Core LIDAR Thomson Scattering diagnostic was upgraded with new detectors. The previously observed discrepancy in the measured electron temperature between the LIDAR and ECE diagnostics [3] was reduced and in many cases eliminated. This prompted an investigation into the JET core LIDAR diagnostics optical design and calibration through ray tracing. In this model the cause of the observed systematic error in the measured electron temperature profiles was determined to be a result of the angular effects on the transmission functions of optical interference filters within the spectrometer. In ray tracing, an analysis of a large number of rays provides a high quality representation of the system during both plasma measurements and the calibration. The developed ray-tracing model looks into the behaviour of the collected light rays on the filter surfaces, namely the distribution of incident angles as a function of position in the plasma. Applying this model along with laboratory measurements of the stray light filters transmission as a function of wavelength and incident angle, generated a change in the spectral calibration of the diagnostic.

2. JET CORE LIDAR LAYOUT

The JET core LIDAR spectrometer is a 6-channel system arranged in a 3D layout, where the channels of the spectrometer are defined by a set of low pass filters arranged in a stack configuration. In this filter stack the collected light is reflected off of the filters as shown in Figure 1, defining the channels of the spectrometer [4]. In all but channel 6, stray light filters were placed just in front of the detector. In order to avoid confusion, the transmission functions of the two types of filters examined in this work, the stray light filters and filter stack filters will be referred to as stray light filters and transmission functions respectively.

Inside the system there are three different stray light filter configurations and two different stray light filter types. In particular, channel 3 contains two stray light filters, one of which is tilted by approximately 25 degrees with respect to the optical axis. Due to the combined effect of the stray light filter type, configuration, and channels proximity to the ruby laser wavelength (694.3nm), channels 2 and 3 were the only channels that the presence of these stray light filters was expected to influence Thomson scattering measurements.

The required transmission characteristics of the stray light filters were obtained using a Lambda9000 UV/VIS spectrophotometer, where the transmission of the stray light filter was measured at 0, 10, 20, and 30 degree light incidence. The measurements at normal incidence were used as the baseline stray light filter function to be modified according to the modelled angular distribution of incident light. The data from the tilted incidence measurements was used to determine the value of the filters effective refractive index (n_{eff}). The effective refractive index is required in determining the effective wavelength shift due to the angle of incidence of the incoming light (θ) given the refractive index of the surrounding medium (n_0), given by equation (1) [7].

$$\lambda \rightarrow \lambda \sqrt{1 - \left(\frac{n_0}{n_{eff}}\right)^2 \sin^2 \theta}. \quad (1)$$

3. N_{eff} CALCULATION

Due to the lack of documentation on these Ruby stray light filters it was necessary to calculate the effective refractive index. To accomplish this, the measured filter transmissions were compared to the shifted baseline stray light filter function at the same angles of incidence 10, 20, and 30 degrees with a varying n_{eff} . These shifted baseline functions were obtained by applying equation 1 to the measured normal incidence stray light filter function for a range of possible n_{eff} values. This fitting process found the optimal value for n_{eff} to be equal to 1.65. In figure 3, the dashed curves all used this value of 1.65 for n_{eff} in the calculation of the shifted distribution for the three angles using equation 1.

4. RAY TRACING MODEL

The few key elements that were necessary in order to perform the necessary ray tracing consist of: the plasma source definition, the modelling of the white light calibration source, and the definition of the stray light filter surfaces. Before the construction of the model it was observed that the different channels of the spectrometer have an identical optical path from the source to the detector (ignoring channel 1). Identifying this feature of the system made it possible to perform all modifications and subsequent ray tracing calculations based on a single channel of the spectrometer.

4.1. SOURCE DEFINITION

To model the light collected from different positions within the plasma, a longitudinal source was defined with bounds extending from $r/a = -0.8$ corresponding to the High Field Side (HFS) to $r/a =$

0.8 corresponding to the Low Field Side (LFS). In the expression r/a , r is the position relative to the major radius and a is the minor radius of the tokamak. The different plasma positions are defined as points along this extended line source.

For the JET core LIDAR system there are six vessel windows where collected TS light is brought outside the vessel and onto the six corresponding mirrors of the vertical mirror assembly. During white light calibration these vessel windows are covered with a screen that is illuminated by a white light source. This in turn illuminates all mirrors of the vertical mirror assembly and the collected light travels through the diagnostics optics to the detectors surface. The calibration setup was modelled as a source plane the same size as one of the vessel windows and on this surface thirteen uniformly distributed point sources were defined. This collection of point sources produced a light distribution similar to the actual system, entirely illuminating the corresponding mirror in the vertical mirror assembly.

4.2. RAY TRACING PROCESS AND RESULTS

The purpose of this model was to capture the expected angular distribution of rays on the stray light filter surfaces for both operation and calibration instances. In the ray tracing process, each ray is individually launched from its defined source point to a point within the detectors surface.⁸ The process is repeated to generate a full spread of rays from the various source points. The incident angle onto the stray light filter surface for each of the traced rays was calculated, resulting in the angular distributions shown in Figure 5.

The angular distributions were calculated for five radial positions in the plasma, along with the distribution captured during the white light calibration of the system. Due to the layout of the system with six collection mirrors with none being on axis there are no points at zero incidence angle for any of the angular distributions in either measurements or calibration. Furthermore, it is clear from Figure 5 that the diagnostics white light calibration was not a good representation of the angular distributions observed during plasma measurements. This difference in the angular distributions during white light calibration and plasma measurements is most pronounced in the core of the plasma. This resulted in the systematic error being largest in the region where the diagnostic is designed to deliver the highest quality measurements as a “Core LIDAR TS diagnostic”. With such severe incidence angles the calibration was not applicable and the affected measurements must be corrected by taking into account these distributions in order to be accurate around the $r/a = 0.0$ position of the plasma.

5. EFFECT OF RAY ANGLES ON FILTER TRANSMISSION FUNCTIONS

Using these angular distributions, the measured normal incidence filter function, and the calculated n_{eff} together with equation 1, the wavelength shift due to ray angles was calculated. In some cases this angular effect caused a substantial shift in the peak transmission range of the stray light filter function downward in wavelength space. In Figure 6 the impact of the ray angles on the stray

light filter function is observed. This shift in the filters transmission affects the spectral calibration of the diagnostic. For channels 2 and 3 of the spectrometer, regions exist where the shifted stray light filter function is not at its peak transmission value for wavelengths where the channels transmission function is defined. In these regions, with the shifted stray light filter function applied to the underlying transmission function, a decrease in the total integrated area of the transmission function is observed. Figure 7 shows how each plasma position resulted in a different level of modification to the underlying transmission function of Ch2 as expected, based on the observed angular distribution at each position.

The integral of each of these curves range from $I_{\text{centre}}/I_{\text{underlying}} = 0.88$ at the central plasma position, to $I_{r/a=0.8}/I_{\text{underlying}} = 0.77$ at the low field position. The transmission function modified by the white light calibrations angular distribution observed the greatest reduction in the integrated area of the channels transmission function, with a ratio of $I_{\text{whitelight}}/I_{\text{underlying}} = 0.74$.

While the results here are for Ch2, Ch3 undergoes the same process. For Ch3, the presence of the 25 degree tilted filter causes the stray light filter function to alter the underlying channel transmission function. Without this tilted filter element there would be no effect on the spectral calibration of Ch3.

6. SYSTEMATIC ERROR CALCULATION

In order to quantify the impact that the modifications to the channel 2 and 3 transmission functions had on plasma measurements, the systematic error within the diagnostic were calculated.

$$T_{\text{underlying}}(\lambda) = f(\lambda, \theta = 0) \quad (2)$$

This calculation started with the white light angular distribution being applied to the underlying transmission function for each channel. This modified the underlying function by reducing its integrated signal area by a factor representative of the stray light filter wavelength shift for that channel.

$$T_{\text{baseline}}(\lambda) = [T_{\text{underlying}}(\lambda, \theta = 0) \times \int T_{\text{WL}}(\lambda, \theta = f_{\text{WL}}()) d\lambda] \quad (3)$$

The white light calibration integral factors of 0.740 for Ch2 and 0.903 for Ch3 were then applied to the underlying transmission of the respected channel; resulting in a new set of baseline transmission functions. The plasma position modified functions were fitted to this new baseline function (T_{baseline}), allowing for the expected T_e and n_e systematic errors to be calculated.

$$T_{\text{measured}}(\lambda) = [T_{\text{underlying}}(\lambda, \theta = 0) \times \int T_{\text{TS}}(\lambda, \theta = f_{\text{TS}}()) d\lambda] \quad (4)$$

From the baseline and measured transmission functions, a value for $T_{e, \text{observed}}$ is calculated by fitting

the signal obtained by T_{measured} for each underlying input temperature ($T_{e, \text{input}}$) to the signal obtained by T_{baseline} . This process simulates the measurement process of the JET LIDAR TS diagnostic, where the signal observed in each channel is compared to its white light calibrated value.

Using the calculated calibration correction factors, the effective T_e systematic error for the diagnostic can be determined. In Figure 8, the systematic T_e ratio of $T_{e, \text{observed}}/T_{e, \text{actual}}$ is plotted.

From the calculation of the systematic T_e error for the various plasma positions it is observed that the observed T_e values are approximately 6–12 % lower than the actual T_e values over the measurable temperature range. The calculation of the systematic error follows a similar pattern, peaking at approximately 10% systematic error at a T_e near 1keV (see figure 10). The large errors observed for both T_e and n_e at values of T_e approaching zero, is due to the diagnostics inability to accurately measure at these low temperature values.

7. CORRECTION OF JET CORE LIDAR TS DATA

Using the calibration correction factors for each of the five plasma positions computed through ray tracing, a linear fit was applied to generate a correction function covering the full spatial range measured by the diagnostic. This correction function was applied to the white light calibration of the diagnostic, adjusting the calibration to account for the ray angle effect on the spectral calibration. On JET there are multiple diagnostics that can measure the T of the core plasma; the core LIDAR TS, Electron Cyclotron Emission (ECE), and High Resolution Thomson Scattering (HRTS) diagnostics [9, 10]. When the developed correction was applied to existing core LIDAR TS data, a substantial increase in the measured electron temperature of the plasma core was observed, bringing it closer into agreement with measurements by the other diagnostics.

The corrected carbon wall JET discharge database was broken up into two groupings, one spanning from Pulse No's: 49800 to 78166 and the other from 78167 to 79853. In the first set, the stray light rejection issue being corrected for interfered with another issue, the partial depolarization of the laser light. This partial depolarization caused an issue with the calibration of channel 1 being the only channel with a polarizer. This resulted in an additional calibration error of approximately 5% in T_e that was not corrected for. In the second set of discharges, channel 1 was excluded from the fit due to its bad signal to noise ratio, while later discovering the polarization issue. Making the second set of shots the primary grouping used to determine the effectiveness of the correction. Additionally, in the ILW campaign shots 80000 to 81500 were exclusively Ohmic discharges with the stray light filters still installed in the system. In the discharges of the second carbon wall grouping and ILW Ohmic discharges, the application of the correction successfully brought the JET core LIDAR T_e measurements into agreement with that of the other diagnostics. A consequence of this is the realization that the observed discrepancy between the JET LIDAR TS and ECE diagnostics was a combined effect and not solely due to the diagnostics weighing of the non-maxwellian bulk electrons on JET [3] differently, as previously thought.

CONCLUSIONS

Ray tracing has shown that the previously unaccounted for effect of the angular distribution of collected light rays on the detector stray light filters was the primary cause for the observed discrepancy in T_e measurements. With the systems optics optimized for collection of light at the centre of the plasma, while severe incident angles with values of over 20° were observed in the white light calibration of the diagnostic. These incident angles caused a shift and subsequent decrease in the channels integrated signal when the shift of the stray light filter function was extreme enough to alter the channels transmission function. The relative signal observed by the calibrated system versus the actual signal from the various plasma positions is the cause of the observed systematic error. Isolating the cause of this discrepancy allowed for the calculation of correction factors for the diagnostics white light calibration. The application of these correction factors saw an increase in the observed T_e , moving the measurements by the JET core LIDAR diagnostic closer into agreement with the HRTS and ECE diagnostics for all applicable JET discharges and in some cases completely removing the discrepancy.

It is expected that a LIDAR system will be used as the ITER Core TS diagnostic. In the ITER system or any other future LIDAR diagnostic, errors like the ones described in this work found in the diagnostics design or its operation must be avoided. In principle, any possible source of error should be properly studied and corrected for. In particular, the use of optical filters in any area where they could affect the diagnostics operation should be avoided.

ACKNOWLEDGEMENTS

The first author would like to acknowledge the contribution added by T. O’Gorman for his ZEMAX macro code, used to extract the necessary ray angle and position data. This work was supported by EURATOM and carried out within the framework of the European Fusion Development Agreement. Additionally, this work was partly funded by the RCUK Energy Programme under Grant EP/I501045, by the ITER-NL Programme and by the European Communities under the Contracts of Association between EURATOM, CCFE, and FOM, respectively. The views and opinions expressed herein do not necessarily reflect those of the European Commission.

REFERENCES

- [1]. G.F. Matthews et al 2011 Physica Scripta **2011** 014001 <http://dx.doi.org/doi:10.1088/0031-8949/2011/T145/014001>
- [2]. G.F. Matthews et al., Journal of Nuclear Materials **438** (2013) S2-S10 <http://dx.doi.org/10.1016/j.jnucmat.2013.01.282>
- [3]. E. de la Luna, V. Krivenski, G. Giruzzi, C. Gowers, R. Prentice, J.M. Travere, and M. Zerbini, Review of Scientific Instruments **74**, 1414 (2003)
- [4]. H. Salzmann, J. Bundgaard, A. Gadd, C. Gowers, K.B. Hansen, K. Hirsch, P. Nielsen, K. Reed, C. Schrödter, and K. Weisberg, Review of Scientific Instruments **59**, 1451 (1988).

- [5]. M. Kempenaars, J. C. Flanagan, L. Giudicotti, M.J. Walsh, M. Beurskens, and I. Balboa, *Review of Scientific Instruments* **79**, 10E728 (2008).
- [6]. C. Gowers, K. Hirsch, P. Nielsen, and H. Salzmann, *App. Optics*, Volume 27, Issue 17 (1988).
- [7]. R. Scannell, M. Beurskens, M. Kempenaars, G. Naylor, M. Walsh, T. O’Gorman, and R. Pasqualotto, *Review of Scientific Instruments* **81**, 045107 (2010).
- [8]. E.L. Dereniak and T.D. Dereniak. (2008). *Geometrical and Trigonometric Optics*. Cambridge University Press.
- [9]. K.V. Beausang, S.L. Prunty, M.J. Walsh, E de La Luna, R. Scannell, M. Beurskens, M. Maslov, I. Balboa and JET EFDA contributors. EFDA–JET–PR(10)05.
- [10]. V. Beausang, S. L. Prunty, R. Scannell, M. N. Beurskens, M. J. Walsh, E. de La Luna, and JET EFDA Contributors, *Review of Scientific Instruments* **82**, 033514 (2011)

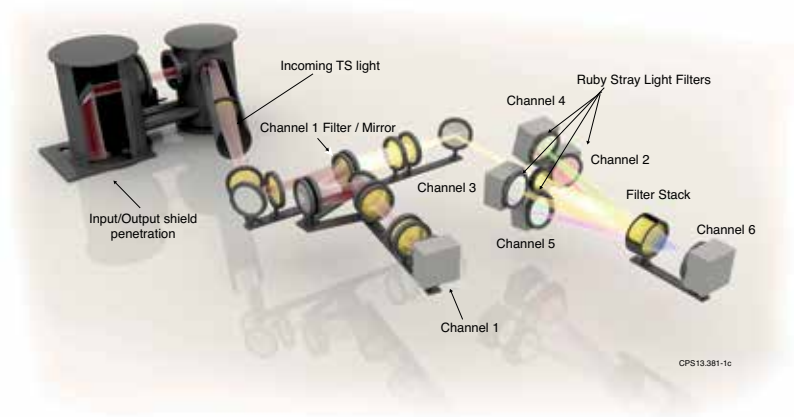


Figure 1: Layout of the JET Core LIDAR Thomson Scattering spectrometer with the channels, filter locations, and light path highlighted. Image is courtesy of EFDA –JET.

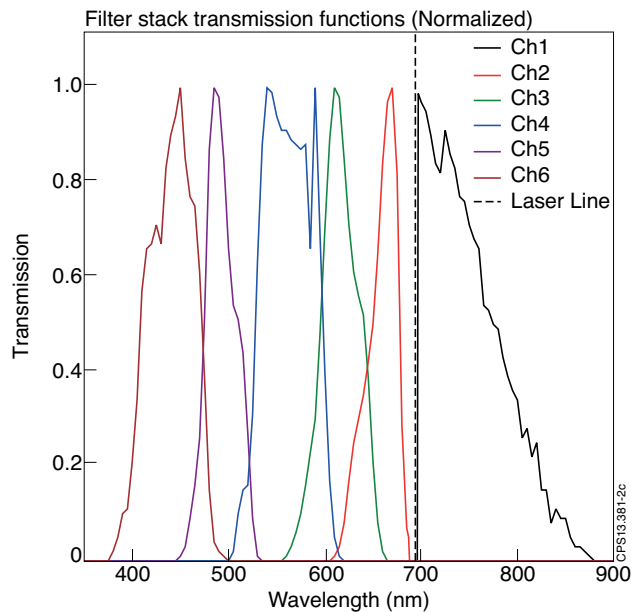


Figure 2: Normalized transmission functions for the JET core LIDAR TS diagnostic generated by the wavelength splitting of the collected light by the low pass filter stack and split into the six channels of the spectrometer.

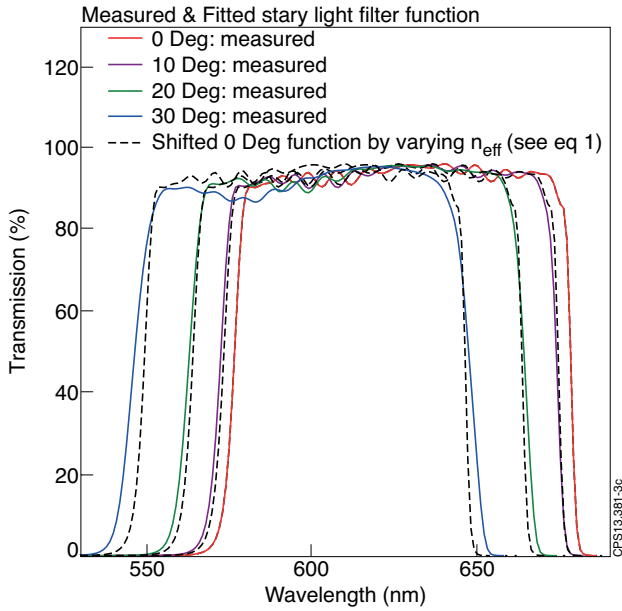


Figure 3: Best fit between the 0 degree transfer function shifted by equation 1 and the measured transfer function for a single fixed nonzero angle of incidence for Ch2 of the JET core LIDAR TS Diagnostic with n_{eff} equal to 1.65.

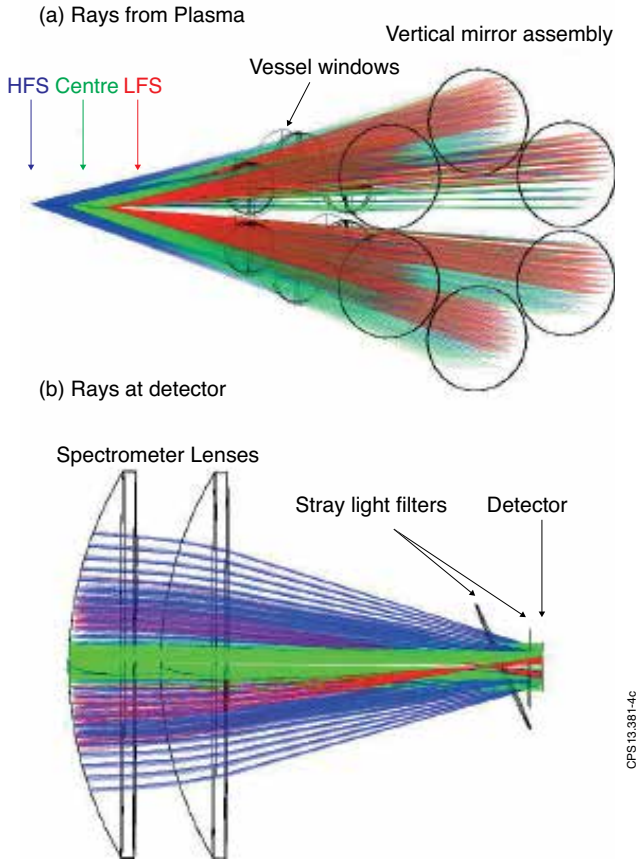


Figure 4: Extended source definition and ray tracing onto the detector for the operational plasma position for the JET LIDAR TS diagnostic.

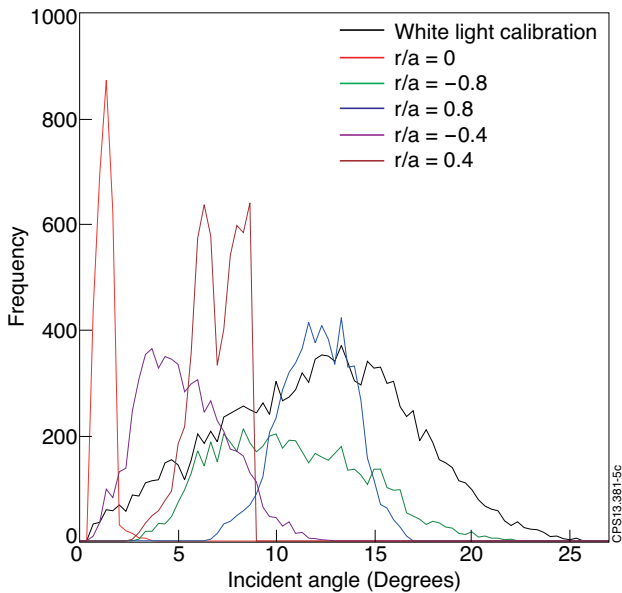


Figure 5: The angular distributions of 6000 rays per plasma position on the stray light filters for the plasma positions and white light calibration cases. These distributions are on a stray light filter placed normal to the optical axis just before the detector.

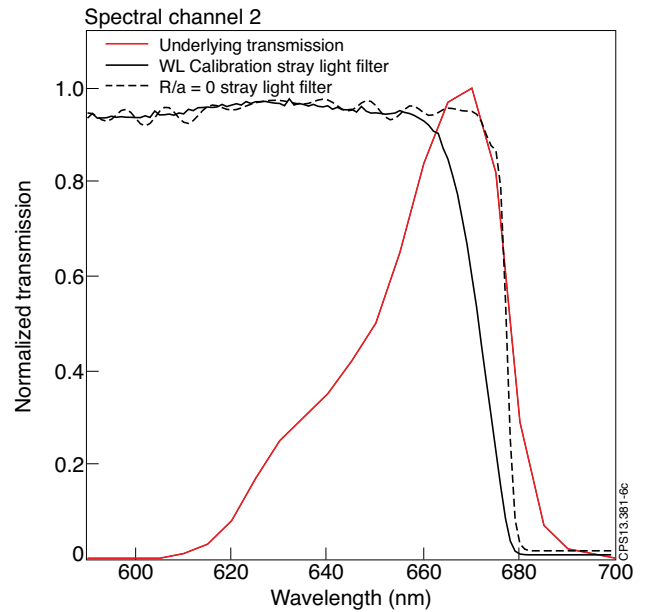


Figure 6: Underlying Ch2 transmission function plotted along with the central plasma position and white light altered stray light filter functions.

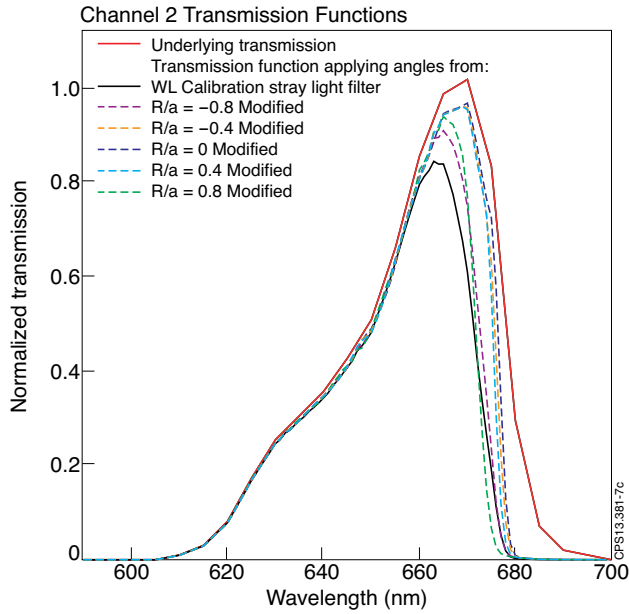


Figure 7: Ch2 underlying transmission function (solid RED), white light modified (solid BLACK), and 5 plasma position modified (Coloured Dashed) transmission functions.

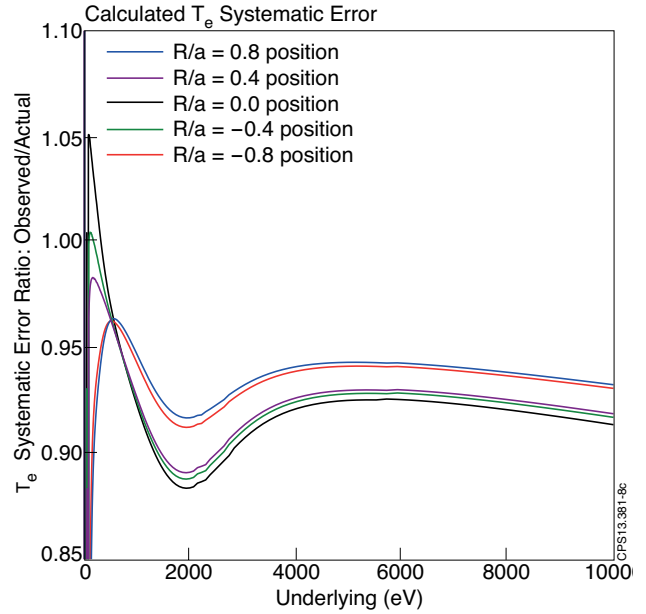


Figure 8: T_e systematic error for the five plasma positions over the entire JET T_e range.

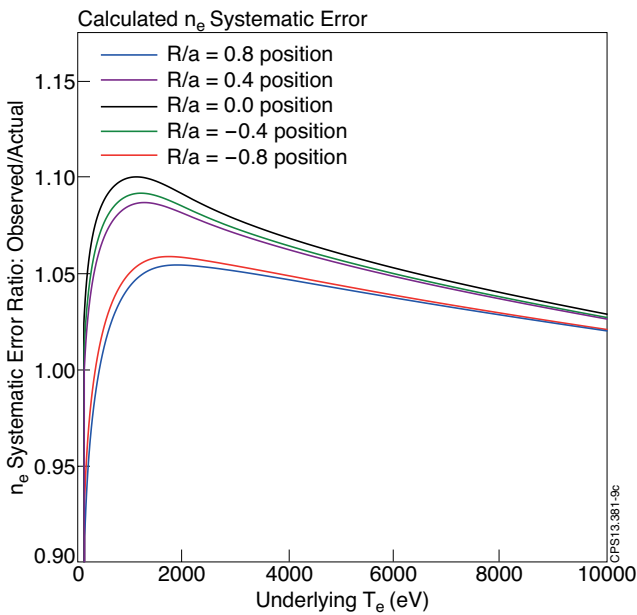


Figure 9: Systematic error in n_e for the five plasma positions over the entire JET T_e range.

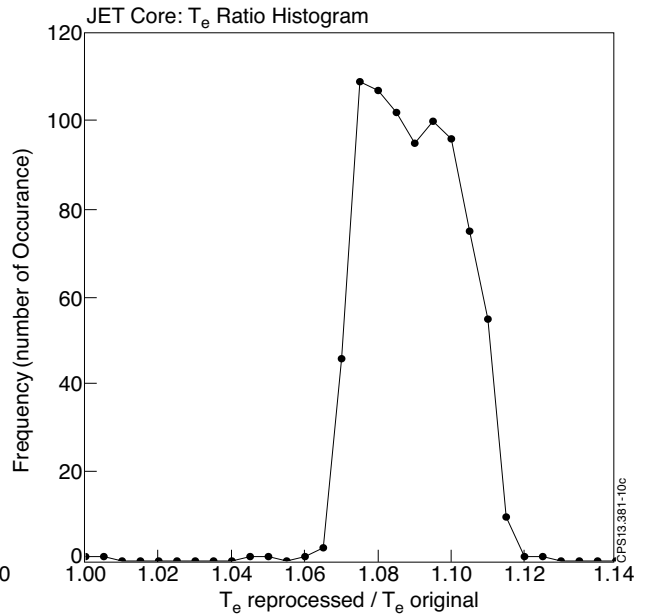


Figure 10: Histogram for the core LIDAR data of the ratio ($T_{e, \text{reprocessed}} / T_{e, \text{actual}}$) for JET Pulse No's: 78167 to 79853.